Supplementary info

High-k gate stacks on low bandgap tensile strained Ge and GeSn alloys for Field Effect Transistors

Stephan Wirths[1], Daniela Stange[1], Maria-Angela Pampillón[1,2], Andreas T. Tiedemann[1], Gregor Mussler[1], Alfred Fox[1], Uwe Breuer[3], Bruno Baert[4], Enrique San Andrés[2], Ngoc D. Nguyen[4], Jean-Michel Hartmann[5], Zoran Ikonic[6], Siegfried Mantl[1] and Dan Buca[1*]*

[1]Peter Grünberg Institute (PGI 9) and JARA-FIT, Forschungszentrum Juelich, 52425, Germany,

[2]Departamento Física Aplicada III: Electricidad y Electrónica, Universidad Complutense de Madrid (UCM), 28040, Madrid, Spain

[3]Central Institute for Engineering, Electronics and Analytics (ZEA), Forschungszentrum Juelich, 52425, Germany

[4]Department of Physics, Solid State Physics - Interfaces and Nanostructures, University of Liege, B-4000, Belgium

[5]Univ. Grenoble Alpes, 38000 Grenoble, France and CEA, LETI, Minatec Campus, 17 rue des Martyrs, 38054 Grenoble, France

[6]Institute of Microwaves and Photonics, School of Electronic and Electrical Engineering, University of Leeds, Leeds LS2 9JT, United Kingdom

*S.wirths@fz-juelich.de, d.m.buca@fz-juelich.de.

1. Growth and strain engineering

Our approach is based on partially relaxed, high Sn content GeSn buffer (SRB) layers for the experimental realization of highly biaxially tensile strained Ge and tensile strained GeSn. The Rutherford backscattering spectrometry (RBS) random and aligned spectra for the $Ge_{0.94}Sn_{0.06}$/Ge/$Ge_{0.89}Sn_{0.11}$ heterostructure are shown in Figure S1. The 10 nm strained Ge layer separates the top tensile strained $Ge_{0.94}Sn_{0.06}$ from the compressively strained $Ge_{0.89}Sn_{0.11}$ buffer allowing RBS analyses like, strain determination, of the topmost layer. The determined channeling minimum yield value χ_{min} of about 5% indicates high single crystalline quality of both the relaxed $Ge_{0.89}Sn_{0.11}$ layer as well as the tensile strained $Ge_{0.94}Sn_{0.06}$. The theoretically achievable strain values in GeSn layers grown on top of 73% relaxed $Ge_{0.9}Sn_{0.1}$ SRB are plotted as a function of the Sn concentration in Figure S1a.

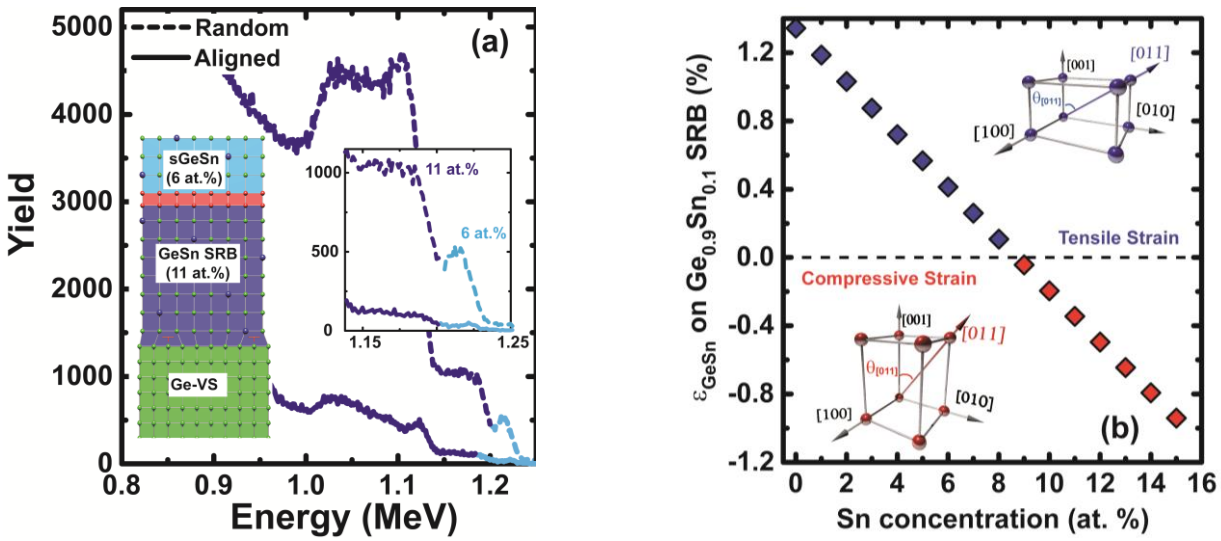

Figure S1: *(a) RBS random and aligned spectra of a strain engineered $Ge_{0.94}Sn_{0.06}$/Ge/$Ge_{0.89}Sn_{0.11}$ heterostructure grown on a Ge-VS. (b) Calculated strain in $Ge_{1-x}Sn_x$ layers grown on $Ge_{0.9}Sn_{0.1}$ buffer layer exhibiting a degree of relaxation of 73%.*

Figure S2a presents the experimentally measured tensile strain in thin Ge layers with thicknesses between 20-50 nm grown on partially strained relaxed $Ge_{1-x}Sn_x$ buffers. Exemplarily, we show in Figure S2b the RSM plot for 50 nm strained Ge with a strain of 1.1% grown on partially relaxed 250 nm $Ge_{0.905}Sn_{0.095}$ buffer on 3 µm thick Ge virtual substrate on Si(100).

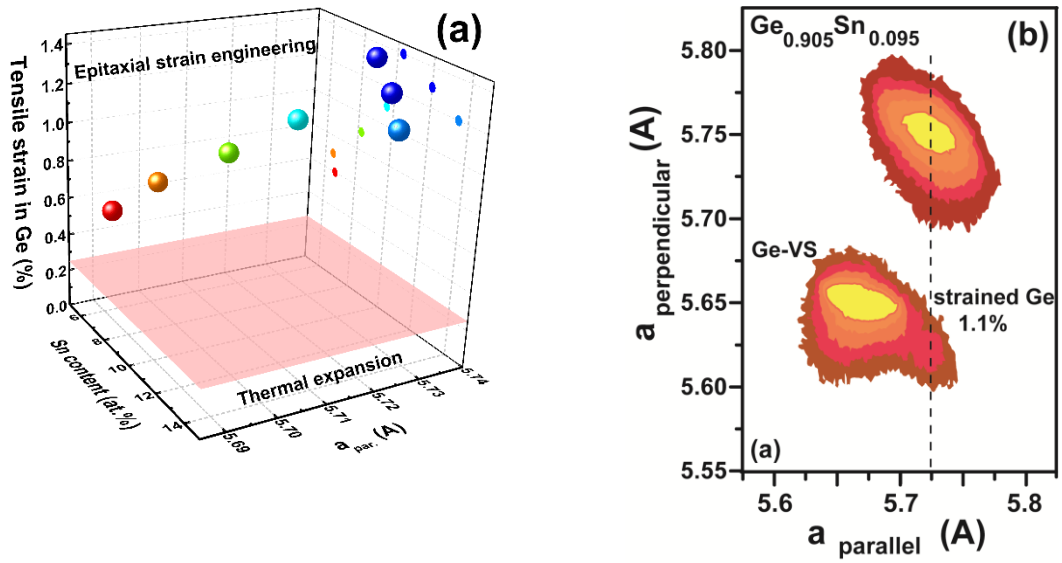

Figure S2 *(a) Experimentally measured tensile strain in Ge layers grown on partially relaxed* $Ge_{1-x}Sn_x$ *buffers. (b) XRD-RSM of 50 nm thick 1.1% strained Ge / 250 nm* $Ge_{0.905}Sn_{0.095}$ *heterostructures.*

2. Oxide deposition

The Al_2O_3 and HfO_2 oxides were deposited in a 300 mm AIXTRON Tricent™ Atomic Layer Deposition tool. The vertical process chamber is equipped with an advanced showerhead designed inlet and temperature controlled side walls. In order to achieve uniform step coverage of the layers the pressure is maintained below 1mbar. Trimethylaluminium (TMA) and Tetrakis Ethylmethylamino Hafnium (TEMAH) precursors for Al and Hf, respectively, are introduces in pulses into the reactor via a Trijet™ evaporator. Pulsed 300 g/m³ O_3 in O_2 is used as oxidizer during deposition process steps as well during the *in-situ* annealing.

The study of low bandgap strained Ge and GeSn alloys requires the use of different temperatures for both dielectric deposition and *in-situ* O_3 oxidation. The experiments presented in this work were performed at 300°C ALD processing.

3. SIMS analyses

SIMS measurements were carried out using a ToF-SIMS IV instrument (IONTOF GmbH). For the mass spectral analysis a pulsed Bi^{3+} beam of 25 keV was used. The beam was raster scanned over an area of 100 x 100 µm. To gain access to the depth distribution of the elements a sputter beam of 1 keV Cs^+ was scanned over an area of 300µm x 300 µm (50nA). The sputtered negative ions were accelerated by 2 keV extraction voltage into the reflectron type drift tube. The single ion counting detection system consisted of a scintillator and a photomultiplier.

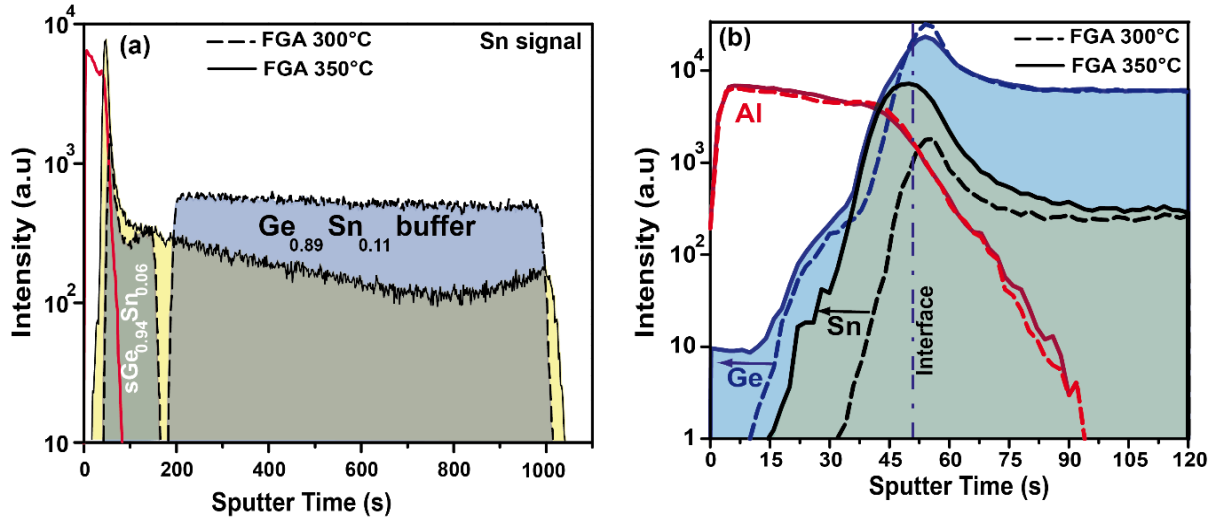

***Figure S3**: The elemental Sn distribution in the Al_2O_3 / $Ge_{0.94}Sn_{0.06}$ / Ge / $Ge_{0.89}Sn_{0.11}$ buffer heterostructures (a) and interface detail (b) after FGA at 300 and 350°C FGA annealing. The O_3 oxidation and the Al_2O_3 deposition were performed at 300°C.*

Figure S3a shows the Sn distribution in the strained $Ge_{0.94}Sn_{0.06}$/Ge/$Ge_{0.89}Sn_{0.11}$ heterostructure after complete MOS capacitor processing. Sharp Sn signal is observed after 300°C forming gas

annealing (FGA) while strong Sn redistribution through the whole structure is clearly visible after 350°C FGA. Details on the atomic Sn and Ge signals at the Al_2O_3 / GeSn interface are shown in Figure S3. At 350°C FGA the Ge atoms diffuses through the Al_2O_3 layer reaching the oxide surface while Sn diffusion stops inside the oxide layer.

4. Band structure calculations

The band structure around the Γ point was calculated by the 8-band k.p method including strain effects[1]. Conduction band valleys, not at the Brillouin-zone center, may split depending on the applied strain as described via appropriate deformation potentials. The parameters used in this calculation are given in Table S1. The alloy parameters are calculated from the corresponding values for Ge and Sn, using Vegard's-type interpolation for the deformation potentials with the quadratic correction (bowing) for band gaps and lattice constant. The exceptions are the Luttinger γ parameters, positive for Ge and negative for Sn, for which the Vegard's law is completely inapplicable. The γ parameters have been calculated in Ref.[2] [2] using the empirical pseudopotential method. These data sets were used here to find a quadratic interpolation formula, which was slightly corrected to reproduce the widely accepted values of Luttinger parameters for pure Ge, given in Table S1, and employed in the calculations. The electron effective mass at the Γ point is not an input parameter, but rather a result from the k.p calculation.

Table S1. *Parameters used in the 8-band k.p method:*

	Ge	**Sn**
Band structure parameters		
a_{latt} (nm)	5.6575	6.4912
γ_1	13.38	-12.0
γ_2	4.24	-8.45
γ_3	5.69	-6.84
E_p (eV)	26.30	23.80
$E_{g,\Gamma}$ (T=0K) (eV)	0.892	-0.408
$E_{g,L}$ (T=0K) (eV)	0.744	0.1202
$E_{g,X}$ (T=0K) (eV)	1.105	0.9102
$\Delta_{s.o.}$ (eV)	0.29	0.70
Deformation potentials at Γ		
a_v	1.24	1.58
b	-2.9	-2.7
a_c	-8.24	-6.0
$T_{0,X}$	636	-

***Table S2**: The bandgap at RT and the minimum electron and hole effective masses for strained Ge and $Ge_{0.94}Sn_{0.06}$ under tensile strain, extracted from Figure 1, main paper. I and D denote the indirect and direct nature of the material, respectively.*

	$Ge_{0.94}Sn_{0.06}$	**Strained Ge**	
Tensile strain	0.4%	1.1%	1.4%
$m_{eff\_electron}$	0.03	0.026	0.024
m_{eff_hole}	0.019	0.024	0.022
Bandgap, E_g	0.569 (D)	0.573 (I)	0.54 (I)

5. Numerical CV characteristics modelling

The numerical modeling software used for the simulation of the heterostructure electrical characteristics is based on the solution of the drif-diffusion semi-classical semiconductor equations. We assume Maxwell-Boltzmann statistics for carrier densities. The expression of the electric current density for electrons is given by

$$J_n = qn\mu_n E + qD_n \nabla n,$$

where the first term corresponds to a drift mechanism of electron transport, with q the electron charge, n the electron concentration, μ_n the electron mobility, E the electric field, and the second term is related to electron diffusion, with D_n the diffusion constant. A similar expression holds for the hole current density. The formal developments are applied to a structure with planar geometry comprising one or several semiconducting layers sandwiched between two metallic electrodes.

The solution to the steady-state regime gives access to all dc properties of the structures, including, as functions the space coordinates for a given value of the applied voltage, the electron and hole concentrations, the electric potential, the electric field and the current densities. In the study of the ac response under small-signal conditions, a sinusoidal electric potential of amplitude $\tilde{V} \ll kT/q$ and of frequency $f = \omega/2\pi$ is added to the steady-state voltage V_0 :

$$V = V_0 + \tilde{V}e^{j\omega t}$$

Within the small-signal approximation, all quantities can be written as the sum of a steady-state term plus a harmonic term. The steady-state and small-signal equations are of similar form; they therefore can be solved along the same numerical procedure. This yields all dc and ac components of the involved physical quantities. The small-signal conductance G and capacitance C are obtained from the complex admittance $Y = \tilde{J}/\tilde{V}$, where $\tilde{J}$ is the complex small-signal amplitude of the total current density. The admittance can be decomposed into an equivalent parallel conductance and capacitance:

$$Y = G(\omega, V_0) + j\omega C(\omega, V_0).$$

Complete C-V characteristics can subsequently be simulated and the influence of the variation of any physical parameters included in the above equations can be observed in a systematic manner. Such an approach notably allows us to probe the role of physical parameters that are not easily experimentally accessible. Complementary details on the numerical procedure can be found in Refs[3,4].

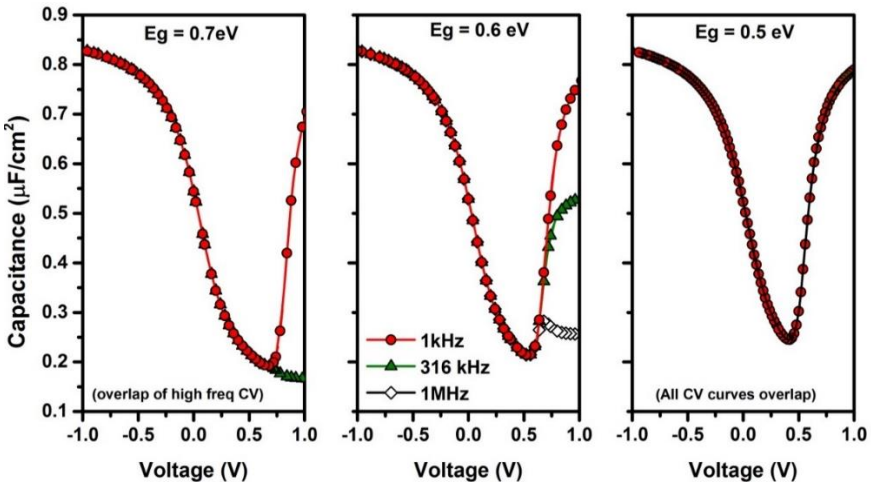

Figure S4: *Effect of bandgap parameter on the frequency response of Al_2O_3/ Ge MOS CV characteristic simulation.*

5. Electrical characterization

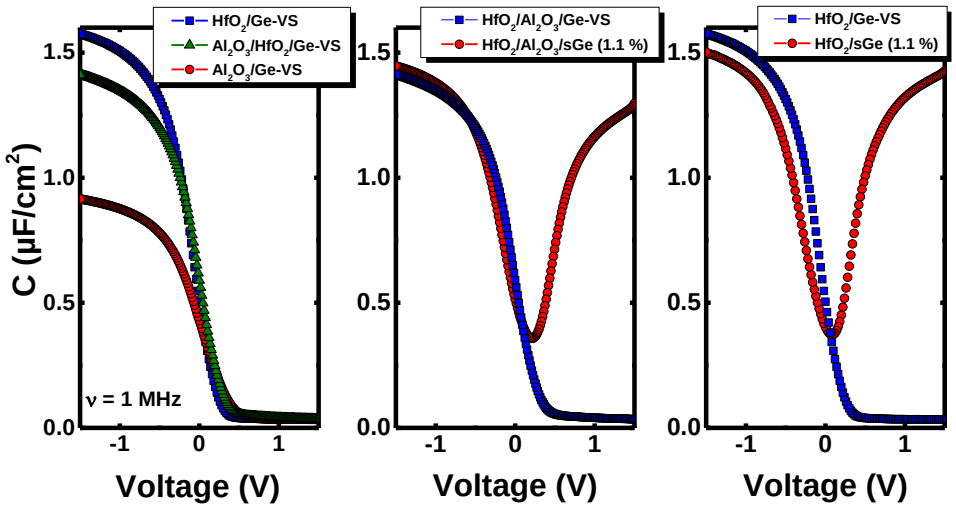

Figure S5: *Comparison of the room temperature CV characteristics for Ge-VS and strained Ge (1.1%) for different high-k gate oxide.*

6. References

(1) Bahder, T. Eight-Band K· p Model of Strained Zinc-Blende Crystals. *Phys. Rev. B* **1990**, *41*, 11992–12001.

(2) Lu Low, K.; Yang, Y.; Han, G.; Fan, W.; Yeo, Y. Electronic Band Structure and Effective Mass Parameters of $Ge_{1-x}Sn_x$ Alloys. *J. Appl. Phys.* **2012**, *112*, 103715.

(3) Baert, B.; Nakatsuka, O.; Zaima, S.; Nguyen, N. D. Impedance Spectroscopy of GeSn-Based Heterostructures. *ECS Trans.* **2013**, *50*, 481–490.

(4) Baert, B.; Schmeits, M.; Nguyen, N. D. Study of the Energy Distribution of the Interface Trap Density in a GeSn MOS Structure by Numerical Simulation of the Electrical Characteristics. *Appl. Surf. Sci.* **2014**, *291*, 25–30.